Chinese Journal of
POLYMER SCIENCE

RESEARCH ARTICLE

https://doi.org/10.1007/s10118-022-2701-9
Chinese J. Polym. Sci. **2022**, *40*, 1016–1027

Facile and One-step Direct Synthesis of Poly(valine) as a Robust Drug Nanocarrier for Enhanced Breast Cancer Therapy

Ya-Bin Meng and Jun Wu*

School of Biomedical Engineering, Sun Yat-sen University, Shenzhen 518107, China

Electronic Supporting Information

Abstract Synthetic poly(amino acid)s with good biodegradable and biocompatible properties have attracted increased attention as carriers in biomedical applications in recent years, their synthesis and purification procedures are usually complicated and some by-products would occur yet. Given this, polypeptide with good biodegradable and biocompatible properties is prepared and optimized by one-step and direct synthesis strategy and poly(valine) (PVal) is selected here as a model polypeptide in this study. This newly generated PVal can self-assemble into poly(valine) nanoparticles (PVal-NPs) with a high drug-loading capacity (>20 wt%) of doxorubicin (DOX) and shows strong cytotoxicity against 4T1 cells. Upon cellular internalization, the release of DOX could be accelerated by the endosomal acidic environment which leads to enhanced anticancer effects. The results *in vivo* show that DOX@PVal-NPs have a long blood circulation time, high cancer accumulation and penetration, and good therapeutic performance in 4T1 tumor-bearing mice without causing obvious adverse effect on main organs. With these combined advantages, these PVal-based nanoplatform would provide an effective drug delivery tool for clinical breast cancer therapy.

Keywords Poly(amino acid); Nanoparticle; Drug carrier; Doxorubicin; Breast cancer

Citation: Meng, Y. B.; Wu, J. Facile and one-step direct synthesis of poly(valine) as a robust drug nanocarrier for enhanced breast cancer therapy. *Chinese J. Polym. Sci.* **2022**, *40*, 1016–1027.

INTRODUCTION

Despite the undeniable advances in recent years, breast cancer developed from local tissue is still one of the deadliest diseases of the current millennium and has been the most commonly diagnosed cancer that threatened the health of people in the latest global survey.[1] Among the breast cancer, triple-negative breast cancer (TNBC) has been one of the most devastating breast cancer along with high metastases and it was the primary cause of poor survival rate in breast cancer patients.[2–4] Improving the therapeutic effect of triple-negative breast cancer needs further clinical and basic studies.[5]

As a traditional anticancer protocol, surgical resection and chemotherapy are routinely performed for TNBC. Regrettably, surgical resection is more traumatic which may induce many complications and incomplete surgical resection can cause tumor recurrence. Chemotherapy is still the main treatment for TNBC, but the use of chemotherapeutic drugs (such as DOX) in clinic has several limitations due to the drug resistance, collateral damages, nonselective distribution and poor penetration.[6,7] Hence, developing a carrier that could solve the above-mentioned obstacles is imperative for TNBC therapy. Recently, nanocarriers include nanoparticles (NPs),[8] liposomes,[9] exosomes,[4] micelles[10] and so on, have been used to deliver chemotherapeutic drugs and shown certain antitumor efficiency on TNBC. Among these platforms, polymeric NPs with good biodegradable properties have been extensively used as drug delivery carrier that hold great advantages,[11] including prolonged blood circulation, improved drug solubility and stability, and delivered chemotherapy drugs to tumors *via* passive or active manner.[12–14] However, their therapeutic efficacy has often been hindered as a result of poor drug loading capacity, limited accumulation and penetration in tumor.[15] And these issues seem to be induced partially by the inappropriate material select and design for drug delivery. Given that, great efforts have been devoted to choosing proper material and systematically designing for the drug carrier.

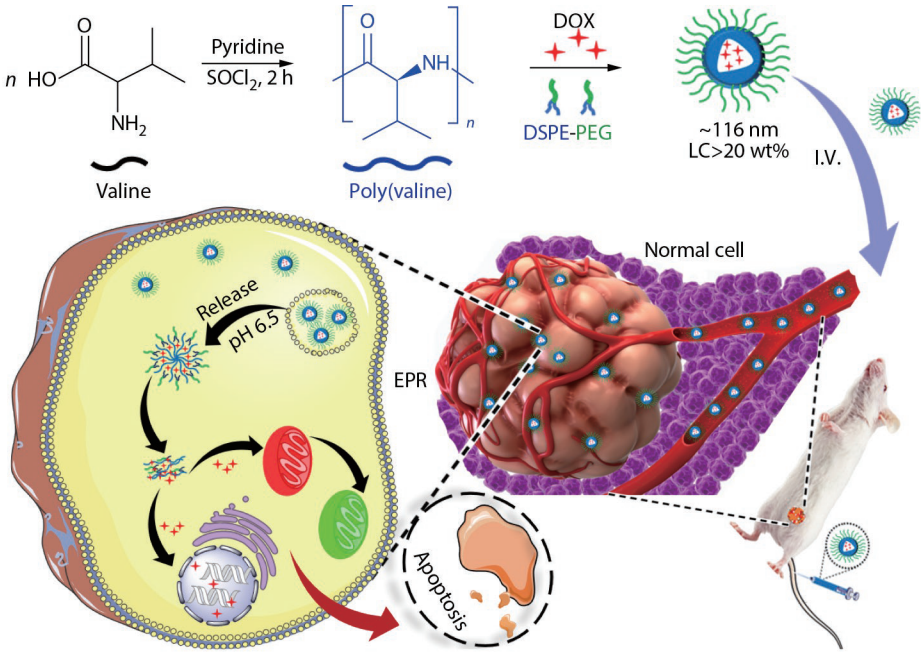
Poly(amino acid)s or polypeptide with good biodegradable and biocompatible properties have been successfully prepared for drug delivery in recent years,[16,17] but their further application has often been hampered as a result of their complicated synthesis and purification procedures.[18]

Aiming to prepare polypeptide easily and directly, valine, one of the 20 basic amino acids, is selected here as a model amino acid to fabricate polypeptide. Following systematic screening, PVal with eight val units is selected as a nanocarrier to encapsulate DOX with poor solubility to generate DOX@PVal-NPs (Scheme 1). 4T1 cells were used as a trial subject to

* Corresponding author, E-mail: wujun29@mail.sysu.edu.cn

Special Issue: Biomedical Polymers
Received December 24, 2021; Accepted January 24, 2022; Published online May 5, 2022

© Chinese Chemical Society
Institute of Chemistry, Chinese Academy of Sciences



Scheme 1 Schematic illustration of the DOX@PVal-NPs platform for systemic drug delivery and tumor therapy.

systematically studied the antitumor effect of DOX@PVal-NPs *in vitro* and *in vivo*. Enhanced anti-cancer efficacy was found in orthotropic breast cancer mice models. Meanwhile, the *in vivo* antitumor efficacy and blood biochemistry revealed a high level of tumor inhibition without inducing obvious side effects on main organs. Given a direct easy-operating but effective synthesis strategy, PVal-NPs could be a flourishing platform for drug delivery and clinical breast cancer therapy.

EXPERIMENTAL

Synthesis of PVal Polymer

In this study, a direct polycondensation method is utilized to prepare PVal by a simple step and thionyl chloride was used as the catalyst. Briefly, $SOCl_2$ (0.72–2.16 mL) was added dropwise into pyridine (10–30 mL) and stirred for 20 min under ice-bath conditions. Subsequently, Val was added and stirred for another 2 h. At the end of the synthesis, organic solvent was removed by rotary evaporation and the prepared product was precipitated in ultra-pure water to remove the monomer and excess organic solvents. After lyophilization, a brown-black powder was obtained.

Preparation of PVal-NPs and DOX@PVal-NPs

Nanoprecipitation was applied to prepare PVal-NPs and DOX/dye@PVal-NPs. Briefly, PVal, DOX/dye and DSPE-PEG_{2000} that dissolved in the DMSO (10 mg/mL) were added dropwise into the water under vigorous stirring (1000 r/min, 30 s). To remove DMSO and free DOX/dye, all the NPs were washed and centrifugated using a centrifugal filter.

Characterization

The physicochemical properties of PVal or NPs were characterized as bellow.

Nuclear magnetic resonance (NMR) spectra

^{1}H-NMR was harnessed to record the chemical structure of PVal and sulfoxide (DMSO-d_6) was used as the solvent. The data were processed by Mestre-Nova software.

Dynamic light scattering (DLS)

The average size and zeta potential were recorded with DLS. The stability of DOX@PVal-NPs over time was carried out in PBS or PBS with 10% FBS and recorded with DLS. All the data were shown as mean±standard deviation (SD).

Drugs loading capability

After washing and centrifugation, NPs with different DOX/PVal ratios were resolved in nine-fold acetonitrile to obtain the DOX loaded in NPs. Following centrifugation (12000 r/min, 10 min), 100 μL of supernatant was collected and the fluorescence of DOX was quantified by using a microplate reader at 480 nm. The calculated formulas were as follows:

$$\text{LC (\%)} = \frac{\text{Weight of DOX loaded}}{\text{Total weight of DOX loaded NPs}} \times 100\% \quad (1)$$

$$\text{EE (\%)} = \frac{\text{Weight of DOX loaded}}{\text{Total weight of DOX added}} \times 100\% \quad (2)$$

In vitro drug release profiles

The release behavior of DOX@PVal-NPs selected after systematic screening was evaluated under predetermined pH media (pH 7.4, 6.8 and 5.5).[19] Briefly, after loading and ultrafiltration, 2 mL of DOX@PVal-NPs that dispersed in the dialysis bags (MWCO 3500 Da) was placed in 20 mL of solution with different pH values under dark environment and stirred constantly in a shaker (37 °C, 100 r/min, ZHWY-200D shaker, China). Subsequently, the release solution (1.0 mL) was drawn out and replaced with fresh medium (1.0 mL) at different time intervals. Finally, DOX that released from DOX@PVal-NPs was measured as aforementioned. All data were described as mean±SD.

Cell Assays

In vitro proliferation

The cytotoxic activity of PVal and drug loaded NPs against 4T1

and 3T3 cells was assessed by CCK8 assay. Cells were split into 96-well plates (5×10^3 cells/well) and cultured for 24 h. Then, DOX, PVal and DOX@PVal-NPs were added into the well at predetermined concentrations. At different time points, 10 μL of CCK8 was added and cultured for 1–2 h and the optical density was recorded at 450 nm.

Cell migration study

After culturation for 24 h, straight lines on 4T1 cell were drawn with a 10 μL sterile pipette tip when cells spread the entire well of the six-well plate. Then, the floating cells were removed and PVal-NPs, DOX@PVal-NPs and DOX that dispersed in medium containing 2% FBS were added to the well, separately. At predetermined time interval (24 and 48 h), cells were photographed and ImageJ software were used to assessed the migration ability of 4T1 cells.

Cell uptake assay

The cell uptake behavior of DOX and DOX@PVal-NPs was assessed and measured by flow cytometer (FCM) and confocal laser scanning microscopy (CLSM). Briefly, 4T1 cells (1×10^5 cells/well) were evenly seeded in glass bottom dishes. After 24 h post seeding, DOX@PVal-NPs was added to the well. At different time points, cells were stained with Hochest33342 and washed with PBS. Finally, cells were fixed and photographed by CLSM. Meanwhile, nanoparticles internalized was quantified by FCM at predetermined time points.

In vitro apoptosis

In this study, cell apoptosis assay was operated to evaluate the apoptosis mediated cell death by flow cytometry analysis.[20] After 24 h post incubating, cells were cocultured with DOX, PVal-NPs and DOX@PVal-NPs at predetermined concentrations and incubated for another 24 h. Then, cells were processed in accordance with the manufacturer's instructions. Finally, cell apoptosis was recorded with FCM.

Hemolysis

The hemolysis assay of PVal-NPs was assessed by a reliable and simple method based on the previous report.[21,22] Briefly, after washing with 0.9% of physiological saline, the red blood cells (RBCs) of SD rats were isolated from serum by centrifugation and then mixed with samples with different concentrations to obtain RBCs with 2% concentration. After 3 h post incubation at 37 °C, the hemolysis of samples was recorded and the rate of hemolysis was calculated as follows:

$$\text{Hemolysis rate (\%)} = \frac{H_{sa} - H_{nc}}{H_{pc} - H_{nc}} \times 100\% \quad (3)$$

where H_{sa}, H_{pc} and H_{nc} are absorbance values of the samples, positive controls (water) and negative control (0.9% physiological saline), respectively.

4T1 orthotopic breast cancer model

The 4T1 orthotopic breast cancer model was made according to a previous report.[8] The mice with a tumor volume reached about 100 mm^3 were randomly divided into four groups (n=5) and used for *in vivo* experiments.

In vivo biodistribution

Since the poor penetration ability of the fluorescence of DOX, the *in vivo* biodistribution of DOX@PVal-NPs was simulated by DiR-loaded PVal NPs according to the previous research.[23] Briefly, 4T1 tumor-bearing mice (n=3) was injected DiR and DiR@PVal-NPs with a DiR concentration of 0.8 mg/kg, respectively. The biodistribution of NPs in the mice was monitored at different time points (1, 2, 4, 8, 12, 24 and 48 h) by using an *in vivo* near infrared fluorescence imaging system. Besides, the accumulation of NPs in major organs (heart, spleen, liver, lung, kidney) and tumors were also evaluated. The spectroscopy parameter of DIR molecules was set at 740/790 nm.

In vivo antitumor efficacy

The biocompatibility and antitumor efficiency of NPs *in vivo* were systematically assessed. Briefly, mice were treated with saline, PVal-NPs, DOX, and DOX@PVal-NPs *via* the tail vein every three days until day 12 and the body weight and tumors size were calculated every other day. The following formula was used to calculate volume: Tumor volume (V, mm^3): $V = L \times W^2/2$, where V is the tumor volume measured at every other day, L is the length of the tumor, W is the width of the tumor.

Serum Biochemistry and Histology

For serum biochemistry, the blood of mice was obtained at the end of the treatment and the biochemical indexes (ALP, AST, ALT, BUN, CRE) were analyzed with a clinical analyzer. In addition, major organs (lung, kidney, heart, spleen, liver) and tumors were also obtained for the histopathological evaluation. Besides, TUNEL was used to assess the therapeutic effect of DOX@PVal-NPs on tumor tissues.

Statistical Analysis

SPSS 17.0 and Origin 8.5 software were applied to analyzed the data. The ANOVA (one-way analysis of variance) and Student's t-test was harnessed to analyze data. All the data were noted as mean±SD. *p<0.05, **p<0.01 and ***p<0.001 considered as the statistical significance or significant differences.

RESULTS AND DISCUSSION

Synthesis and Characterization of PVal

In this study, a facile and one-step direct synthesis method was used to prepare PVal (Scheme 1). The corresponding acyl chloride was first synthesized with thionyl chloride ($SOCl_2$) as the catalyst in the pyridine solvent and then reacted with the amino group ($-NH_2$) of Val. After purification and vacuum drying, a brown-black powder was collected. And an alkaline environment that pyridine provided was used to promote the reaction in the forward direction.

The structure of PVal was characterized by ^{1}H-NMR, low-resolution mass spectrometry and FTIR. As seen in the ^{1}H-NMR spectrum (Fig. 1a), the peak at 7.92 ppm is the hydrogen proton of amide bond of PVal. The peaks at about 2.10 and 1.0 ppm are the hydrogen proton in methylene and methyl of PVal, respectively. According to the FTIR spectrum (Fig. S1 in the electronic supplementary information, ESI), the band at 3286 cm^{-1} is the absorption of —NH—, and 1650 cm^{-1} is the amine I bond (—CO—NH—), indicating that PVal was prepared successfully. As shown in Fig. 1(b), the molecular weight of the PVal ranges from 589 g/mol to 1081 g/mol. After systematic screening and purification, PVal with 8–9 Val units was chosen in this experiment. As mentioned earlier, PVal was successfully polymerized by this direct one-step synthesis strategy.

https://doi.org/10.1007/s10118-022-2701-9

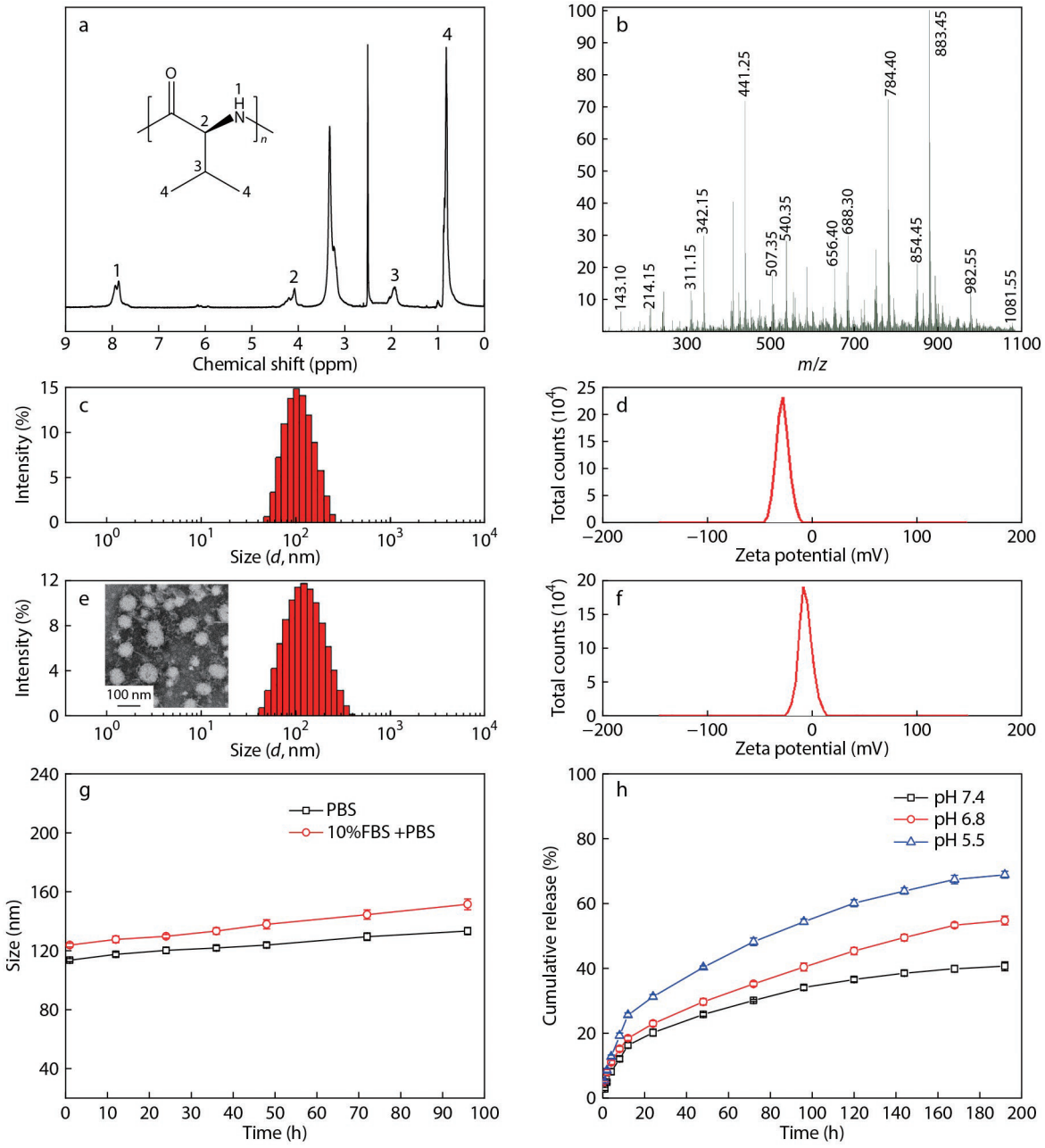


Fig. 1 The characterization of PVal, PVal-NPs and DOX@PVal-NPs. (a) ^{1}H-NMR of PVal; (b) the molecular weight of PVal; Size distribution (c) and zeta potential (d) of PVal-NPs; Size distribution, TEM image (e) and zeta potential (f) of DOX@PVal-NPs. (g) Stability of DOX@PVal-NPs; (h) Cumulative release profiles of DOX from DOX@PVal-NPs.

Preparation and Characterization of PVal-NPs and DOX@PVal-NPs

In this study, nanoprecipitation was harnessed to prepare PVal-NPs and drug/dye@PVal-NPs. As shown in Figs. 1(c) and 1(d), PVal with DSPE-PEG$_{2000}$ as stabilizer could self-assemble into PVal-NPs (~104 nm, −30.1 mV). DOX was selected to generate DOX@PVal-NPs with the size of 110–140 nm and zeta potential ranges from −5 mV to −25 mV (Figs. 1e and 1f). And the morphology of DOX@PVal-NPs is spherical in shape (Fig. 1e). Then the size, zeta potential, encapsulation efficiency (EE) and loading capacity (LC) of DOX@PVal-NPs with different drug and PVal ratios are recorded in Table S1 (in ESI). The LC (%) ranges from 4.29% to 20.49%. The zeta potential increases with the increase ratio of drug and PVal, which may be due to the electrostatic adsorption between the carboxyl in PVal and amine in the DOX. Following systematic screening, DOX@PVal (10:4) with high DOX loading (22.49%) and small size was used in the experiment. As shown in Fig. 1(g), there is almost no obvious change in the particle size of DOX@PVal-NPs over 96 h in both media (PBS or PBS with 10% FBS). Then, the release behavior of DOX from DOX@PVal-NPs under different physiological conditions was also evaluated. As shown in Fig. 1(h), DOX released from DOX@PVal-NPs is relatively fast due to the small NP size, small molecular weight and slow dissolving of

https://doi.org/10.1007/s10118-022-2701-9

polymers. The results above showed that DOX@PVal-NPs with high drug loading capacity were prepared successfully and it may have a pH-dependent drug release.

Cell Assay

To evaluate the mechanism of nanoparticles on the tumor cell, some cellular evaluation, such as cell uptake, CCK8, 3D tumor penetration assay, lysosomal escape and migration assay was carried out.

In vitro cell uptake and penetration assay

The cell uptake efficiency of 4T1 cells treated with DOX@PVal-NPs at different time points was evaluated by CLSM and FCM. As exhibited in CLSM image (Fig. 2a), the cellular internalization of DOX@PVal-NPs presents time-dependent behaviors and the cellular internalization of DOX@PVal-NPs increases correspondingly with the incubation time. Similarly, the uptake of NPs by the cells detected by FCM (Figs. 2b and 2c) is consistent with the results of CLSM and the fluorescence intensity is higher at 8 h (p<0.001). The cell uptake assay indicated that 4T1 cells could internalize DOX@PVal-NPs efficiently. In addition, 3D tumor spheroid assay was applied to indirectly assess the distribution and the penetrability of DOX and DOX@PVal-NPs on tumor tissue. The results display that DOX@PVal-NPs have a better penetrability in tumor spheroids than DOX with poor

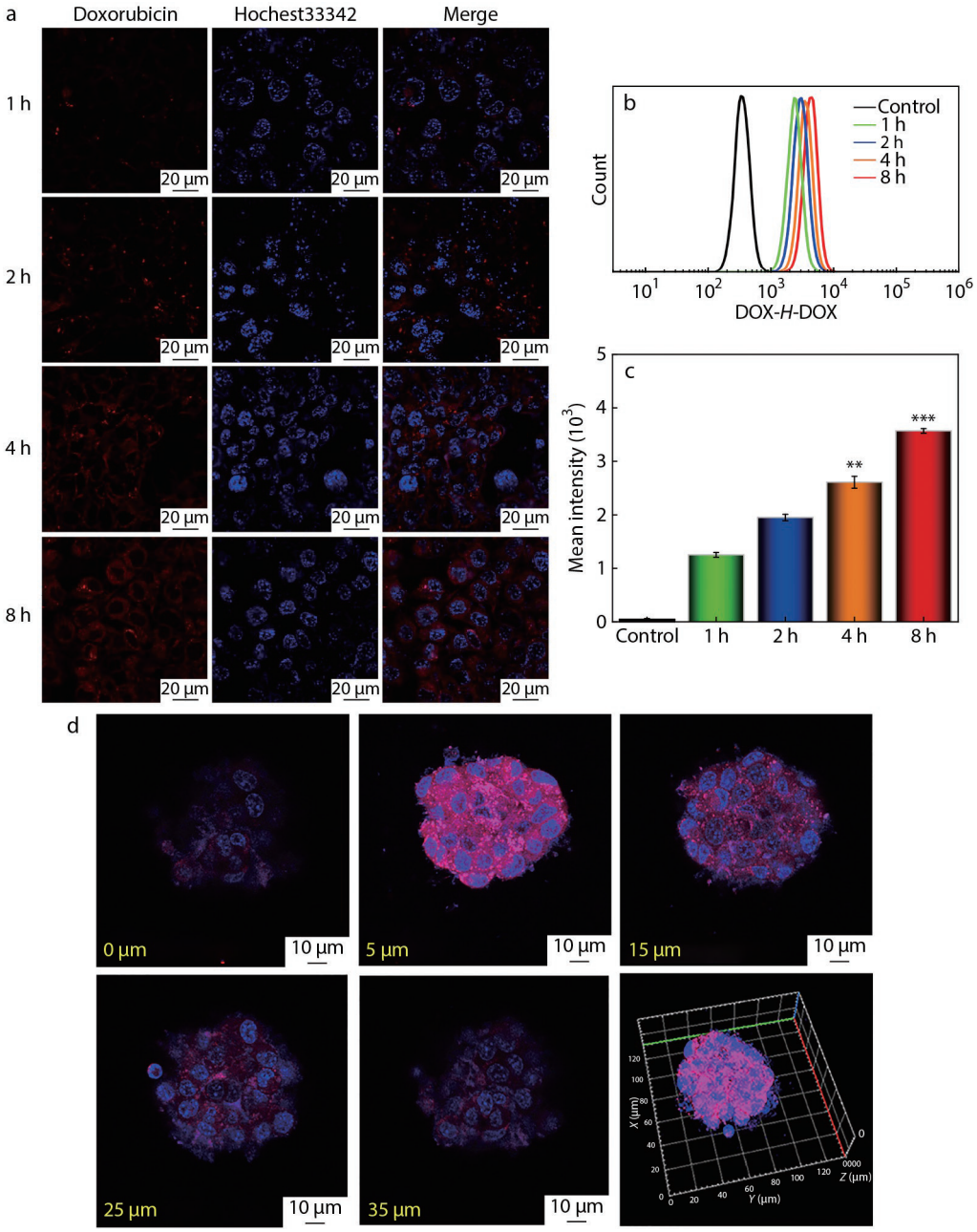


Fig. 2 *In vitro* cell uptake of 4T1 cells incubated with DOX@PVal-NPs. (a) qualitative analysis and (b, c) quantitative analysis, **p<0.01, ***p<0.001; (d) The penetration ability of DOX@PVal-NPs through tumor tissues was assessed by the 3D tumor penetration assay, scale bar=10 μm.

https://doi.org/10.1007/s10118-022-2701-9

penetrability. Thus, PVal could improve the penetration of chemotherapeutic drugs (Fig. 2d and Fig. S3 in ESI).

Bioactivity evaluation and lysosomal escape ability of NPs in vitro

Since DOX could block the synthesis of RNA and DNA, the efficiency of DOX internalization determines the cytotoxicity on tumor cells. In view of this, after treated with PVal-NPs, DOX and DOX@PVal-NPs, the proliferation of 3T3 and 4T1 cells was measured by CCK-8 assay. As seen in Fig. 3(a) and Fig. S2 (in ESI), none of PVal with different concentrations seems to cause obvious cytotoxicity on 4T1 and 3T3 cells. Both free DOX and DOX@PVal-NPs could suppress the cell viability of 4T1 cell in a dose-dependent manner. Encouragingly, due to the enhanced cell uptake and fast release DOX in the tumor cells with lower pH, DOX@PVal-NPs show better antitumor activity than free DOX (Fig. 3b).

Following transportation crossing cytomembrane barriers,

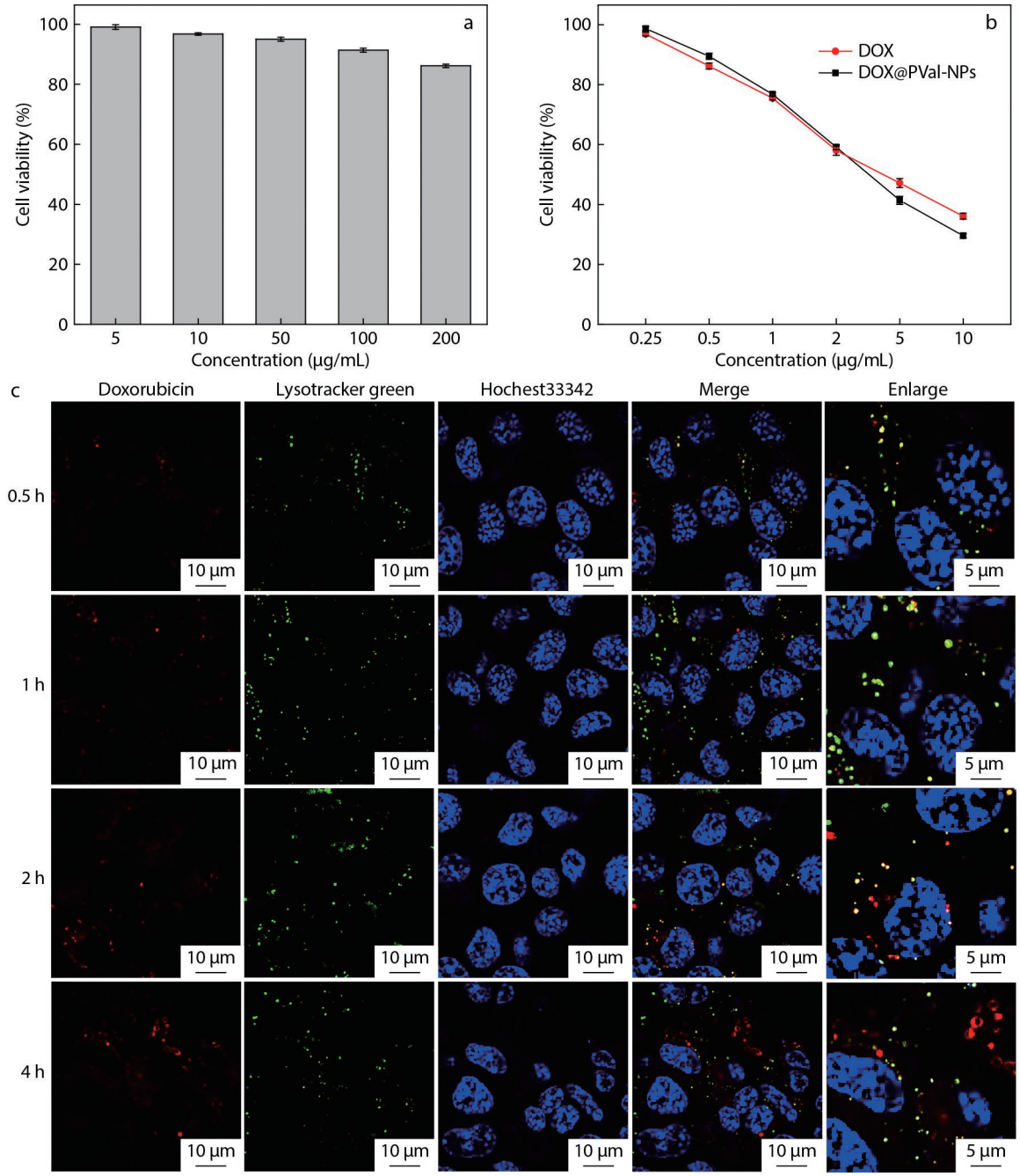


Fig. 3 Bioactivity evaluation and lysosomal escape ability of NPs *in vitro*. (a) The cell viability of 4T1 cells treated with PVal at different concentrations; (b) Cell viability of 4T1 cells treated with DOX and DOX@PVal-NPs; (c) Lysosomal escape assay of 4T1 cells treated with DOX@PVal-NPs (red) for 0.5, 1, 2 and 4 h, scale bar=10 μm. Nuclei and lysosomes were stained with Hoechst 33342 (blue) and Lysotracker green (green), respectively.

https://doi.org/10.1007/s10118-022-2701-9

it is necessary to assess whether DOX@PVal-NPs could escape from the lysosomes and play its antitumor behavior. To verify this, the lysosomal escape ability of DOX@PVal-NPs was evaluated. As shown in Fig. 3(c), the red fluorescence was observed in 4T1 cells after coincubation with DOX@PVal-NPs for 1 h and it could overlap with the green fluorescence of lysosomes within 2 h. After that the overlap begin separate over time, indicating the lysosomal escape of NPs. The result above suggests that PVal-NPs could effectively deliver DOX into cancer cells and escape from the lysosomes.

The in vitro apoptosis mechanism

Once escaping from lysosomes, it is necessary to evaluate whether the DOX@PVal-NPs could cause apoptosis like free DOX. For the study of apoptosis mechanism, FCM was used to quantitatively evaluate the apoptosis of 4T1 cells treated with PVal-NPs, DOX@PVal-NPs and DOX (5 μg/mL) for 24 h. As shown in Fig. 4(a), both DOX and DOX@PVal-NPs groups could induce the apoptosis of 4T1 cells, but DOX@PVal-NPs was the better one. The reason for this was that DOX@PVal-NPs could be internalized effectively by 4T1 cells and exerted antitumor effect

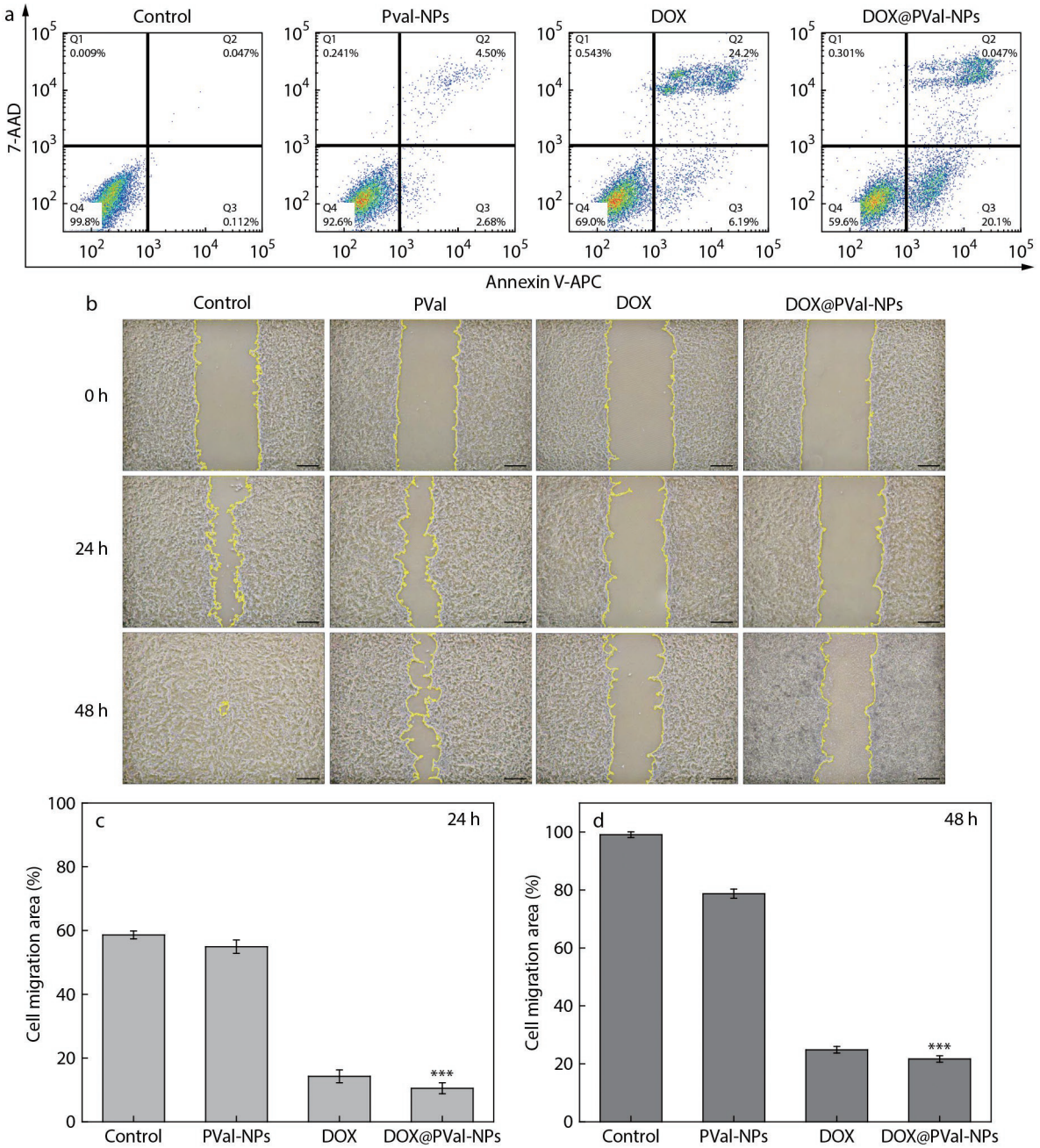


Fig. 4 The *in vitro* apoptosis mechanism of 4T1 cells treated with PVal, DOX and DOX@PVal-NPs for different time points. (a) The apoptosis of 4T1 cells treated with PVal, DOX and DOX@PVal-NPs for 24 h; (b) The migration ability of 4T1 cells treated with PVal-NPs, DOX and DOX@PVal-NPs for 24 and 48 h with different concentration of DOX measured by scratch test, scale bar=100 μm; (c) and (d) were the quantitative analysis of migration ability of 4T1 cells, ***p<0.001.

https://doi.org/10.1007/s10118-022-2701-9

in the tumor cells. In order to more intuitively evaluate the tumor inhibition of DOX@PVal-NPs, 4T1 cells that treated with PVal-NPs, DOX and DOX@PVal-NPs for 24 h was measured by scratch test (Figs. 4b–4d). As shown in the picture, DOX@PVal-NPs show a better inhibition effect on 4T1 cells than free DOX which was in line with the results above.

Biodistribution

Inspired by the *in vitro* antitumor efficiency, the therapeutic effect of DOX@PVal-NPs for *in vivo* therapy was evaluated systematically. Since DOX@PVal-NPs would be finally injected intravenously into body, the successive biodistribution of them *in vivo* should be recorded (Fig. 5). After 2 h post-injection, DiR@PVal NPs could be observed obviously in the tumor site.

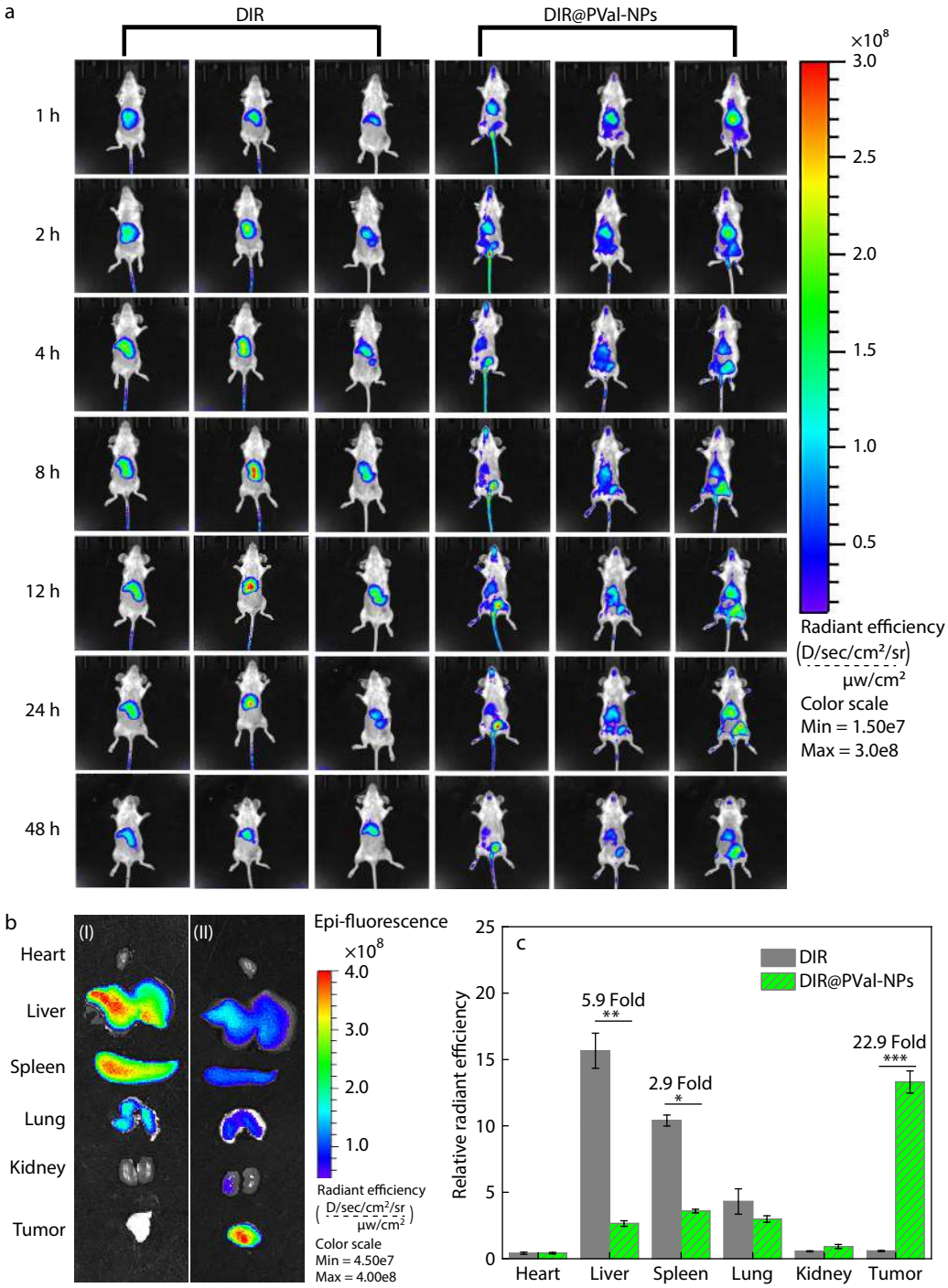


Fig. 5 The biodistribution of NPs *in vivo*. (a) *In vivo* biodistribution of DIR and DIR@PVal-NPs (DIR 0.8 mg/kg) in 4T1 tumor-bearing mice at different time point (n=3); (b) The fluorescence images of primary organs and tumors extracted from mice, (I) and (II) were DIR and DIR@PVal-NPs group, respectively; (c) Quantitative analysis of the fluorescent signals in the major organs and tumors (n=3); *p<0.05, **p<0.01, ***p<0.001

https://doi.org/10.1007/s10118-022-2701-9

More and more DiR@PVal NPs accumulate at the tumor site over time *via* the EPR effect. Although both free DiR and DiR@PVal-NPs could accumulate in liver and spleen inevitably due to the existence of reticuloendothelial system (RES), DiR@PVal-NPs could decrease their accumulation in the normal tissue, prolong their blood circulation time and eventually increase their accumulation at the tumor site (p<0.001).

Evaluation of the Antitumor Activity *In vivo*

With the above promising results *in vitro* and better biodistribution *in vivo*, we further assessed the antitumor effect by *i.v.* injecting saline, PVal-NPs, DOX and DOX@PVal-NPs in 4T1 tumor bearing mice (DOX 5 mg/kg). As shown in Fig. 6(a), tumor growth is notably inhibited in groups treated with DOX and DOX@PVal-NPs (p<0.001) when compare with the saline treated

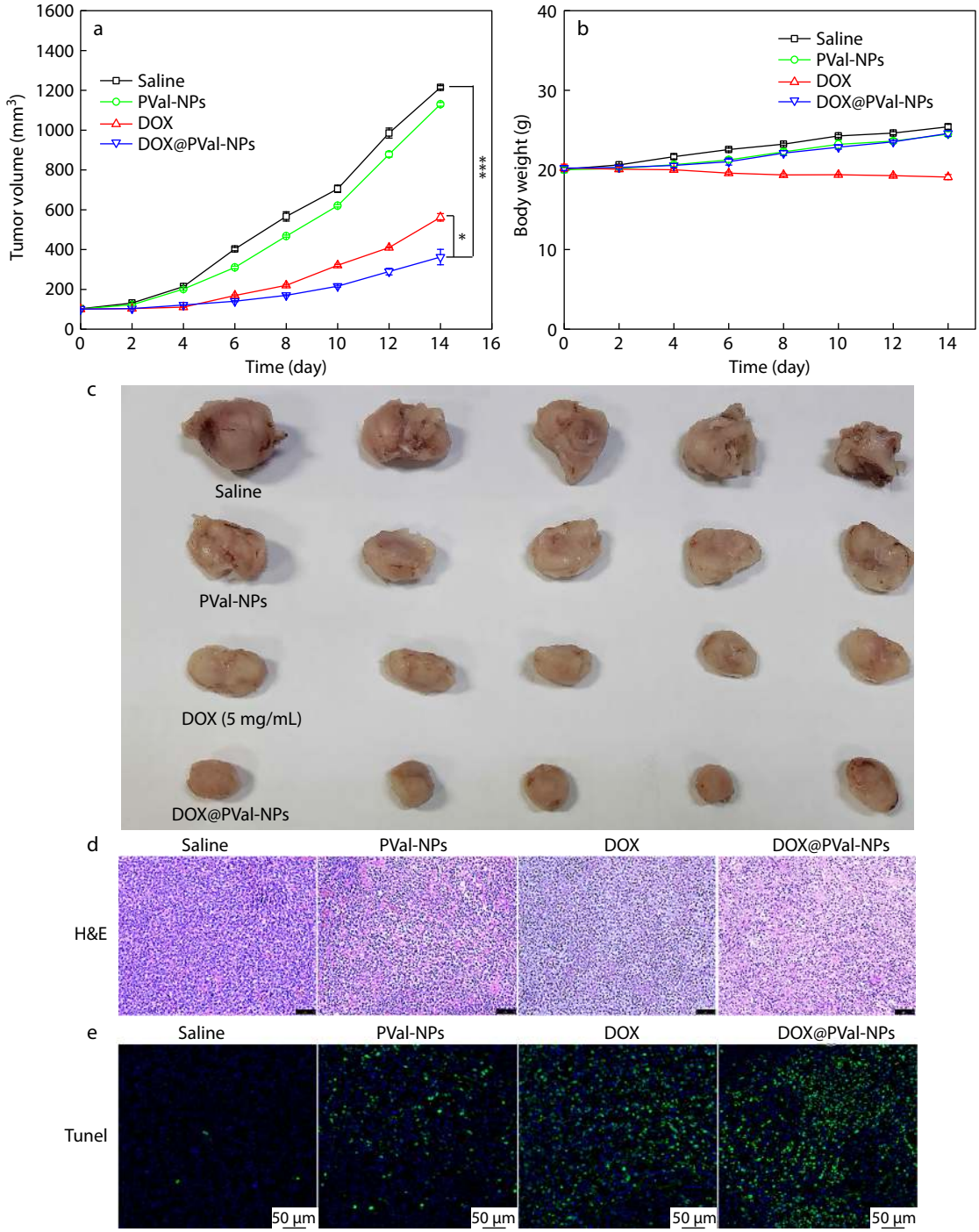


Fig. 6 The *in vivo* antitumor efficacy was studied with 4T1-bearing BALB/C mice which treated with saline, PVal-NPs, DOX or DOX@PVal-NPs *via* the tail vein. (a) Tumor volume, *p<0.05, ***p<0.001; (b) The body weight; (c) Images of gross solid tumors excised at day 14; The (d) H&E (scale bar=75 μm) and (e) TUNEL images (scale bar=50 μm) for the tumor of the mice after treatment with saline, PVal-NPs, DOX (5 mg/kg) or DOX@PVal-NPs (equal concertation to DOX).

https://doi.org/10.1007/s10118-022-2701-9

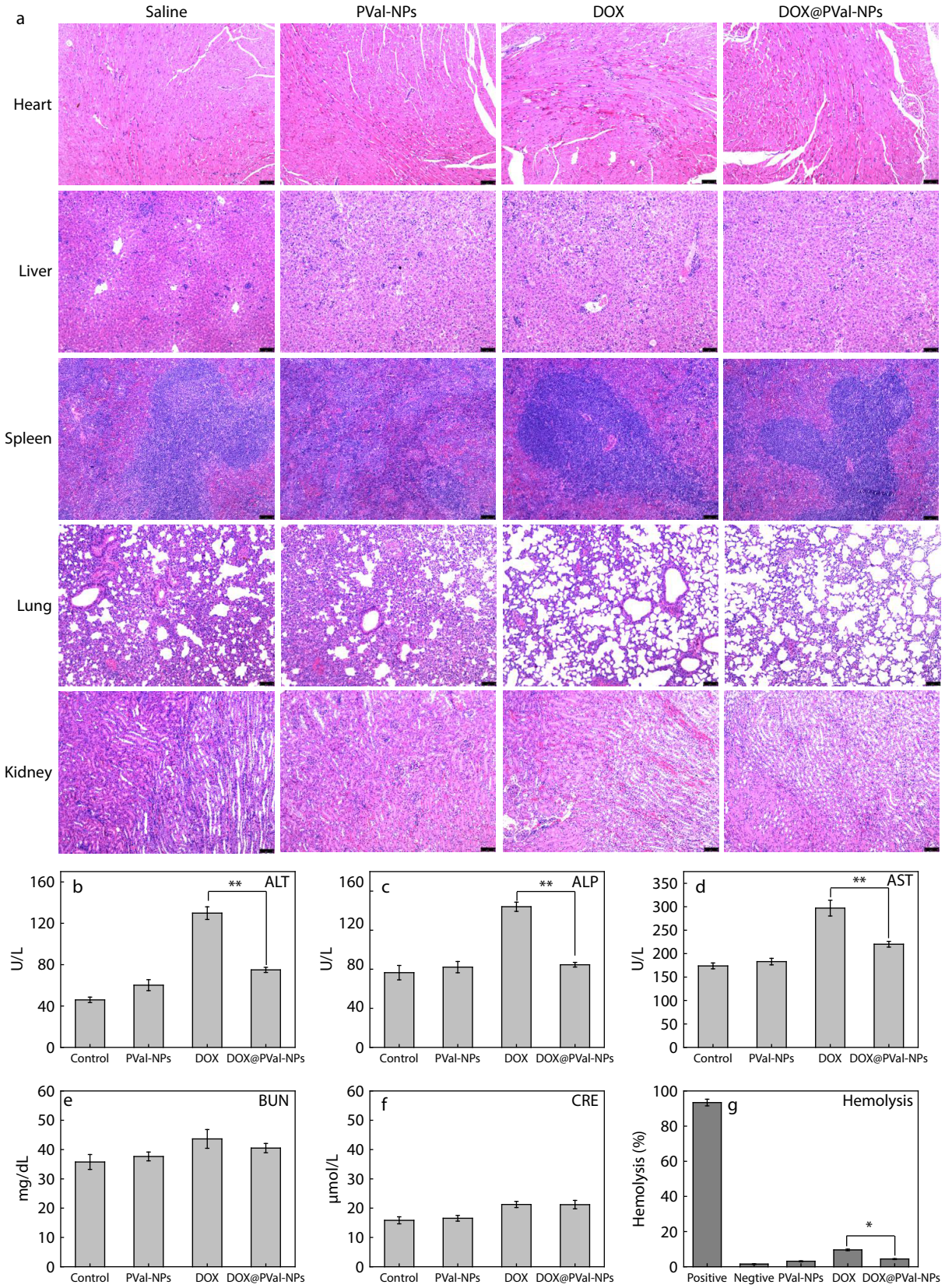


Fig. 7 (a) H&E images for the tissue of tumor-bearing mice after treatment with saline, PVal-NPs, DOX and DOX@PVal-NPs for 14 days, scale bar=75 μm; Serum levels of (b) ALT, (c) ALP, (d) AST, (e) BUN, (f) CRE. (g) The hemolysis of DOX and DOX@PVal-NPs (equal concertation to DOX); (*p<0.05, **p<0.01 versus Control).

https://doi.org/10.1007/s10118-022-2701-9

group. Encouragingly, DOX@PVal-NPs show higher tumor growth suppression than that of free DOX, which could be due to the good tumor accumulation and penetration of DOX@PVal-NPs in the tumor site. The free DOX group achieves a certain effect on tumor inhibition, yet is accompanied by a continuous weight loss during therapy (Fig. 6b) when compared with DOX@PVal-NPs group with enhanced anticancer activity and less impact on the quality of life. Fig. 6(c) shows the comparation of tumor volume which could intuitively present the antitumor efficiency and the result is consistent with Fig. 6(a). As depicted in Fig. S4 (in ESI), Dil@PVal-NPs show a better penetration ability and accumulation than free Dil in the tumor site, which agrees with the *in vitro* 3D tumor spheroids assay (Fig. 3d). In addition, the metabolism of DOX@PVal-NPs *in vivo* was evaluated by pharmacokinetics assay. Compared with the free DOX group, DOX@PVal-NPs exhibite a 3.51-fold higher $t_{1/2}$, a 4.88-fold higher $AUC_{0\text{-inf}}$ and a slower decay in plasma (Fig. S5 in ESI). Besides, compared with the DOX group with insufficient therapeutic effects, DOX@PVal-NPs with a long blood circulation enhance tumor accumulation and penetration ability induced obvious tumor necrosis such as nucleoplasm atrophy and nuclear rupture (Fig. 6d). Encouragingly, TUNEL assay also shows that DOX@PVal-NPs could effectively promote the cleavage of nucleic acids, demonstrating an enhanced anti-tumor therapy *in vivo*, which is in line with the H&E staining assay (Fig. 6e).

Encouraged by the promising antitumor efficiency *in vitro/in vivo*, the biocompatibility of NPs *in vivo* was systematically evaluated by H&E, blood biochemistry and hemolysis. As evidenced in Fig. 7(a), PVal-NPs and DOX@PVal-NPs groups have no obvious toxic on the normal organs as compared with the saline group. However, an evident toxicity (such as inflammation, hyperemic and swelling) on some main organs can be observed in the DOX group. Then, some alterations in related toxicity indicators (ALP, ALT, AST, BUN and CRE) in plasma were assessed. As shown in Figs. 7(b)–7(f), DOX@PVal-NPs reduce the adverse reactions of free DOX. The hemolysis assay shows that DOX@PVal-NPs groups have a negligible hemolysis (<5%) as compared with DOX (p<0.05) (Fig. 7g and Fig. S6 in ESI).

CONCLUSIONS

In this study, a facile one-step synthesis strategy is used to construct PVal with different Val units. Following systematic screening, PVal with eight Val units was selected in this experiment. This newly generated NP platform possesses a high drug load capacity (>20 wt%), high stability under normal physiological conditions and strong cytotoxicity against 4T1 cells. The evaluation of DOX@PVal-NPs *in vitro* and *in vivo* were systematically studied by cellular uptake, anticancer efficacy and systemic toxicity. The *in vivo* results indicate that DOX@PVal-NPs have a long blood circulation time, high tumor accumulation and penetration ability, and good therapeutic performance without causing obvious systemic toxicity associated with DOX. Given an easy-operating and effective strategy is used to prepare poly(amino acid), PVal-NPs could be a flourishing platform for drug delivery and clinical breast cancer therapy.

NOTES

The authors declare no competing financial interest.

Electronic Supplementary Information

Electronic supplementary information (ESI) is available free of charge in the online version of this article at http://doi.org/10.1007/s10118-022-2701-9.

ACKNOWLEDGMENTS

This work was financially supported by the National Natural Science Foundation of China (No. 51973243), International Cooperation and Exchange of the National Natural Science Foundation of China (No. 51820105004), Guangdong Innovative and Entrepreneurial Research Team Program (No. 2016ZT06S029), the Science and Technology Planning Project of Shenzhen (No. JCYJ20190807155801657).

REFERENCES

1 Sung, H.; Ferlay, J.; Siegel, R. L.; Laversanne, M.; Soerjomataram, I.; Jemal, A.; Bray, F. Global cancer statistics 2020: GLOBOCAN estimates of incidence and mortality worldwide for 36 cancers in 185 countries. *CA Cancer J. Clin.* **2021**, *71*, 209–249.
2 Nanda, R.; Chow, L. Q. M.; Dees, E. C.; Berger, R.; Gupta, S.; Geva, R.; Pusztai, L.; Pathiraja, K.; Aktan, G.; Cheng, J. D.; Karantza, V.; Buisseret, L. Pembrolizumab in patients with advanced triple-negative breast cancer: phase Ib KEYNOTE-012 study. *J. Clin. Oncol.* **2016**, *34*, 2460–2467.
3 da Silva, J. L.; Nunes, N. C. C.; Izetti, P.; de Mesquita, G. G.; de Melo, A. C. Triple negative breast cancer: a thorough review of biomarkers. *Crit. Rev. Oncol./Hematol.* **2020**, *145*, 102855.
4 Li, S.; Wu, Y.; Ding, F.; Yang, J.; Li, J.; Gao, X.; Zhang, C.; Feng, J. Engineering macrophage-derived exosomes for targeted chemotherapy of triple-negative breast cancer. *Nanoscale* **2020**, *12*, 10854–10862.
5 Schmid, P.; Adams, S.; Rugo, H. S.; Schneeweiss, A.; Barrios, C. H.; Iwata, H.; Dieras, V.; Hegg, R.; Im, S. A.; Wright, G. S.; Henschel, V.; Molinero, L.; Chui, S. Y.; Funke, R.; Husain, A.; Winer, E. P.; Loi, S.; Emens, L. A.; Investigators, I. M. T. Atezolizumab and Nab-Paclitaxel in advanced triple-negative breast cancer. *New Engl. J. Med.* **2018**, *379*, 2108–2121.
6 Fan, J. L.; Liu, B.; Long, Y.; Wang, Z.; Tong, C. Y.; Wang, W.; You, P. D.; Liu, X. M. Sequentially-targeted biomimetic nano drug system for triple-negative breast cancer ablation and lung metastasis inhibition. *Acta Biomater.* **2020**, *113*, 554–569.
7 Zhang, H.; Fei, J. B.; Yan, X. H.; Wang, A. H.; Li, J. B. Enzyme-responsive release of doxorubicin from monodisperse dipeptide-based nanocarriers for highly efficient cancer treatment *in vitro*. *Adv. Funct. Mater.* **2015,** *25*, 1193-1204.
8 Xiong, F.; Ling, X.; Chen, X.; Chen, J.; Tan, J.; Cao, W.; Ge, L.; Ma, M.; Wu, J. Pursuing specific chemotherapy of orthotopic breast cancer with lung metastasis from docking nanoparticles driven by bioinspired exosomes. *Nano Lett.* **2019**, *19*, 3256–3266.
9 Guo, P.; Yang, J.; Liu, D. X.; Huang, L.; Fell, G.; Huang, J.; Moses, M. A.; Auguste, D. T. Dual complementary liposomes inhibit triple-negative breast tumor progression and metastasis. *Sci. Adv.* **2019**, *5*, eaav5010.
10 Zhang, Y. J.; Zhu, X.; Chen, X. L.; Chen, Q. J.; Zhou, W. X.; Guo, Q.; Lu, Y. F.; Li, C.; Zhang, Y.; Liang, D. H.; Sun, T.; Wei, X. B.; Jiang, C. Activated platelets-targeting micelles with controlled drug

release for effective treatment of primary and metastatic triple negative breast cancer. *Adv. Funct. Mater.* **2019**, *29*, 1806620.
11 Ding, J.; Chen, J.; Gao, L.; Jiang, Z.; Zhang, Y.; Li, M.; Xiao, Q.; Lee, S. S.; Chen, X. Engineered nanomedicines with enhanced tumor penetration. *Nano Today* **2019**, *29*, 100800.
12 Tao, W.; Zeng, X. W.; Wu, J.; Zhu, X.; Yu, X. H.; Zhang, X. D.; Zhang, J. X.; Liu, G.; Mei, L. Polydopamine-based surface modification of novel nanoparticle-aptamer bioconjugates for *in vivo* breast cancer targeting and enhanced therapeutic effects. *Theranostics* **2016**, *6*, 470–484.
13 Wolfram, J.; Ferrari, M. Clinical cancer nanomedicine. *Nano Today* **2019**, *25*, 85–98.
14 Meng, Q. S.; Meng, J.; Ran, W.; Wang, J. Y.; Zhai, Y. H.; Zhang, P. C.; Li, Y. P. Light-activated core-shell nanoparticles for spatiotemporally specific treatment of metastatic triple-negative breast cancer. *ACS Nano* **2018**, *12*, 2789–2802.
15 Shi, J.; Kantoff, P. W.; Wooster, R.; Farokhzad, O. C. Cancer nanomedicine: progress, challenges and opportunities. *Nat. Rev. Cancer* **2017**, *17*, 20–37.
16 Zhang, Y. J.; Sun, T.; Jiang, C. Biomacromolecules as carriers in drug delivery and tissue engineering. *Acta Pharm. Sin. B* **2018**, *8*, 34–50.
17 Schnaider, L.; Brahmachari, S.; Schmidt, N. W.; Mensa, B.; Shaham-Niv, S.; Bychenko, D.; Adler-Abramovich, L.; Shimon, L. J. W.; Kolusheva, S.; DeGrado, W. F.; Gazit, E. Self-assembling dipeptide antibacterial nanostructures with membrane disrupting activity. *Nat. Commun.* **2017**, *8*, 1365.
18 Deming, T. J. Synthesis of side-chain modified polypeptides. *Chem. Rev.* **2016**, *116*, 786–808.
19 Zhong, P.; Qiu, M.; Zhang, J.; Sun, H.; Cheng, R.; Deng, C.; Meng, F.; Zhong, Z. cRGD-installed docetaxel-loaded mertansine prodrug micelles: redox-triggered ratiometric dual drug release and targeted synergistic treatment of B16F10 melanoma. *Nanotechnology* **2017**, *28*, 295103.
20 Wan, G. Y.; Cheng, Y. Y.; Song, J.; Chen, Q.; Chen, B. W.; Liu, Y. Y.; Ji, S. L.; Chen, H. L.; Wang, Y. S. Nucleus-targeting near-infrared nanoparticles based on TAT peptide-conjugated IR780 for photo-chemotherapy of breast cancer. *Chem. Eng. J.* **2020**, *380*, 122458.
21 Zhou, H.; Lv, S.; Zhang, D.; Deng, M.; Zhang, X.; Tang, Z.; Chen, X. A polypeptide based podophyllotoxin conjugate for the treatment of multi drug resistant breast cancer with enhanced efficiency and minimal toxicity. *Acta Biomater.* **2018**, *73*, 388–399.
22 Tao, J.; Dang, M.; Su, X. D.; Hao, Q.; Zhang, J. J.; Ma, X. B.; Lu, G. M.; Zhang, Y. L.; Tian, Y.; Weng, L. X.; Teng, Z. G.; Wang, L. H. Facile synthesis of yolk-shell structured monodisperse mesoporous organosilica nanoparticles by a mild alkalescent etching approach. *J. Colloid Interface Sci.* **2018**, *527*, 33–39.
23 Meng, F.; Wang, J.; Ping, Q.; Yeo, Y. Quantitative assessment of nanoparticle biodistribution by fluorescence imaging, revisited. *ACS Nano* **2018**, *12*, 6458–6468.

https://doi.org/10.1007/s10118-022-2701-9